Radiation Physics and Chemistry 184 (2021) 109437

Contents lists available at ScienceDirect

Radiation Physics and Chemistry

journal homepage: www.elsevier.com/locate/radphyschem

X-ray spectra and gamma factors from 70 to 120 kV X-ray tube voltages

Guillermo Eduardo Campillo-Rivera [a,*], Carina Oliva Torres-Cortes [a], Joel Vazquez-Bañuelos [a], Mayra Guadalupe Garcia-Reyna [a], Claudia Angelica Marquez-Mata [b], Marcial Vasquez-Arteaga [c], Hector Rene Vega-Carrillo [d]

[a] Programa de Doctorado en Ingenieria y Tecnologia Aplicada, Unidad Academica de Ingenieria Electrica, Universidad Autonoma de Zacatecas, Av. Lopez Velarde 800, Col. Centro, 98000, Zacatecas, Zac, Mexico
[b] TecNM/Instituto Tecnologico de Aguascalientes, Av. Adolfo Lopez Mateos 1801 Ote., Frac. Bona Gens., 20256, Aguascalientes, Ags, Mexico
[c] Universidad Sr de Sipán, Chiclayo, 14000, Peru
[d] Unidad Académica de Estudios Nucleares, Universidad Autonoma de Zacatecas, Ciprés 10, Fracc. La Peñuela, 98060, Zacatecas, Zac, Mexico

ARTICLE INFO

Keywords:
X-rays
Spectra
Air kerma
Ambient dose equivalent
Gamma factors
Monte Carlo

ABSTRACT

The energy distribution of photons (spectrum) produced in X-ray generators, or X-ray tubes, depends on current, voltage and the target/filter combination; in turn, the dose depends on the spectrum. During the X-ray tube operation, the dose is due the direct beam or useful beam, the leaking out from the X-ray unit, and those photons scattered by the patient. The dose rate must be reduced to allowable limits using a shielding. In the shielding design an important parameter is the dose normalized to the current and the time, that in this work we named Gamma factor, as the factor used for gamma-ray sources. In this work analog Monte Carlo methods were used to calculate the photon spectra and the Gamma factors for air-Kerma and the Ambient dose equivalent for 70, 80, 90, 100 and 120 kV X-ray tubes having tungsten target and aluminum filter. The mean energies of photon spectra were calculated and the conversion coefficients for H*(10) and Ka per unit fluence were calculated and compared with the coefficients for monoenergetic photons. The glass enclosure and the filter eliminate the low-energy photons; calculated spectra show the continuous X-ray distribution due to Bremsstrahlung and the discrete distribution, due to characteristics X-rays. Photon fluences and doses depend on the X-ray unit voltage. Both gamma factors are similar to values recommended in norms while the fluence-to-dose (Ka and H*(10)) conversion coefficients in function of the mean energy are larger than the fluence-to-dose conversion coefficients for monoenergetic photons.

1. Introduction

Around us there are natural and artificial ionizing radiation sources that contribute to radiation exposure. Natural radiation sources include radioisotopes in the earth, water, air, food and radiation due to cosmic rays. Artificial radiation sources are produced in anthropogenic activities such as: energy production, mining, biology, forensics, medicine etc. The largest source of exposure is the use of radiation sources in medicine (Omori et al., 2020; Blakely, 2000; Webster, 1995).

In magnetic resonance imaging, ultrasound, X or γ-ray imaging the patient is exposed to radiation sources; some are no-ionizing while another are ionizing. The image is a power tool to improve the diagnosis, to follow up the evolution of a medical treatment or to help the treatment planning. Therefore, the image quality is important; unfortunately the image quality is compromised by the equipment technology and the technician's experience and expertise. In radiology the X-ray systems are in constant development, thus machine learning algorithms have been developed to improve the efficiency in the detection of small lesions (Willemink et al., 2020; Campillo-Rivera et al., 2019).

Radiological techniques include conventional radiographs, computed tomography (CT), positron emission tomography (PET), mammography and dental radiography. Micro focal, digital and real time techniques are advanced radiographic methods having better image definition and faster image processing improving the capability of detecting small defects. X-ray images allow a faster and cheaper diagnosis being in growing demand contributing to the exposure to ionizing radiation in the population (Teles et al., 2020; Vazquez-Bañuelos, 2019).

ALARA (As Low As Reasonably Achievable) is a basic principle of

* Corresponding author. UaIN – Universidad Autonoma de Zacatecas, Av. Lopez Velarde # 800, Col. Centro, 98000, Zacatecas, Zac, Mexico.
E-mail address: guillermo_campillo_rivera@hotmail.com (G.E. Campillo-Rivera).

https://doi.org/10.1016/j.radphyschem.2021.109437
Received 27 October 2020; Received in revised form 3 March 2021; Accepted 11 March 2021
Available online 17 March 2021

radiation protection where time, distance and shielding are combined to reduce the radiation exposure. In radiation shielding the thicknesses of walls, ceiling and floor (barriers) are calculated in order to reduce the radiation levels. Barriers of halls having X-ray equipment for diagnosis must be calculated to reduce the dose due to the direct X-ray beam as well as the dose due to X-rays that leak-out from the X-ray unit and the dose due to X-rays scattered-out from the patient body. Thus, the dose outside the barriers must be as low as the weekly permissible dose for radiation workers or for the public (Holroyd, 2018; Okunade, 2005; NCRP, 2004).

For occupational exposed individual or radiation worker the annual Effective dose limit based on stochastic effect is 50 mSv/year. Including the restriction of 100 mSv in 5 years the average annual dose limit is 20 mSv/year. For shielding design the allowable weekly dose limit at any area can be defined in terms of operational or radiation protection quantities (ICRP, 1991; NCRP, 1993; ICRP, 1996; NCRP, 2004; Okundade, 2005; NOM, 2006) or in terms of Air Kerma (Ka) under the condition that the annual Effective dose limit is fulfilled.

In shielding design the areas to be protected are defined as Controlled and Uncontrolled whose weekly dose limit are 0.1 mSv/week and 0.02 mSv/week for dose equivalent respectively. In terms of Ka the limits are 0.1 mGy/week and 0.02 mGy/week for controlled and uncontrolled areas respectively. The voltage, and its rectification, filters and the target angle modifies the air-kerma rate; in the aim to determine de Ka. Lopez Gonzalez et al. (2016) measured the spectra of 40–150 kV X-ray tubes of secondary and transmitted photons. Also, Santos et al. (2016) measured the X-ray spectra for 50–150 kV X ray generators. In both works the X-ray tubes have a tungsten target and with the spectra the Ka-to-H*(10) ratios were obtained and reported in terms of the spectra mean energy. Katho et al. (2011) measured this parameter in X-ray tubes with tungsten target varying the voltage and the thickness of aluminum filter.

During operation the X-ray tube there are three sources of radiation: primary (Pri), leakage (L) and the scattered radiation (Sca) by the irradiated object (patient). The total dose rate per radiographic image (Δ_T) in the occupied area due to these three sources is $\Delta_T = \Delta_{Pri}+\Delta_{Sca}+\Delta_L$. These doses are scaled up to the facility workload. Each source must be analyzed in the aim to calculate the shielding thickness to reduce it to allowable dose rate limits (Okunade, 2005; NCRP, 2004; NCRP, 2003).

In X-ray analytical techniques, radiological protection and radiation dosimetry is important to know the X-ray spectra; these can be calculated or measured. Calculations are carried out using deterministic or Monte Carlo methods (Poludniowski, 2007; Boone, 1998).

Birch and Marshall (1979) developed a semiempirical model to calculate the X-ray spectra from 30 to 150 kV, calculated spectra were also measured with a Ge(Li) and NaI(Tl) detectors. Boone (1998) developed a parametric model to define the X-ray beam quality. Bath et al. (1998) did compare the X-ray spectra calculated by different computational procedures with measured spectra.

The use of Monte Carlo methods to calculate the X-ray spectra allows to use complex geometries and to track the transport of electrons, and secondary particles. Some Monte Carlo-based codes, like EGS4, MCNP, BEAMnrc, and ITS has been used to calculate the X-ray spectra produced by mammography X-ray tube with different combinations of target and filter (Ay et al., 2004) and for 150 kV x-ray tube (Rodriguez-Ibarra et al., 2016).

Monte Carlo codes has been also used to compare the spectra obtained by deterministic codes like SpekCalc (Poludniowski et al., 2009) or to evaluate the performance of different procedures to unfold the X-ray spectra (Shafahi et al., 2020). Also, Monte Carlo codes has been developed to calculate the X-ray spectra from units with different purposes to image diagnosis like energy dispersive spectrometer attached to a scanning electron microscope (Gauvin et al., 2006; Gauvin and Michaud, 2009; Cheol-Ha et al., 2018).

Due to the wide use of Monte Carlo methods to determine the X-ray spectra for therapy and diagnostic Medical Physics several recommendations to report the results have been provided (Sechopoulos et al., 2015, 2018).

Recently, Omar, Andreo and Poludniowski (2020a) developed an analytical model for bremsstrahlung production. In their model were included the electron distribution and the bremsstrahlung angular distribution. Later, the enhanced their analytical model including the production of characteristic X-rays. Their model was validated by comparing their results with other analytical models, experimental data and Monte Carlo calculations (Omar, Andreo and Poludniowski, 2020b).

X-rays are produced in the target (anode), mainly around the focal spot, through the collimator, and passing through the filter, the primary X-ray beam is directed toward the patient and the image receptor. The dose rate, per radiography, from this primary radiation source (Δ in mGy or in mSv), which is function of the operational voltage, is directly proportional to the X-ray current (I in mA) and the exposure time (t in minutes) and inversely proportional to square of the distance between the focal spot to the occupied area (d in meters) as is shown in equation (1).

$$\Delta = \Gamma_\Delta \frac{I\ t}{d^2} \tag{1}$$

In equation (1) Γ_Δ is the Gamma factor for the dosimetric quantity Δ to 1 m from the focal spot, in mGy-m^2 o mSv-m^2 per mA-minute. This Gamma factor is alike to the dose rate constants defined for point-like gamma-ray sources (Smith and Stabin, 2012; Pibida et al., 2008; Ninkovic et al., 2005; Wasserman and Groenwald, 1988; Ungar and Truby, 1982). The Γ_Δ factor is also named Output of constant potential of the X-ray generator to 1 m from the target (ICRP, 1982).

The objective of this work was to estimate the X-ray spectra for X-ray tubes and to calculate the Gamma factor in terms of Air Kerma (Γ_{Ka}) and the Ambient dose equivalent ($\Gamma_{H^*(10)}$). Calculations were carried out to X-ray tubes working to 70, 80, 90, 100 and 120 kV with tungsten target and aluminum filter. Also, the fluence-to-Ka and the fluence-to-H*(10) conversion coefficients were calculated and compared with the conversion coefficients for monoenergetic photons.

For external radiation the dose coefficients, also named fluence-to-dose conversion coefficients, link the operational and the protection quantities to radiation fluence (Dewji and Hertel, 2019).

Conversion coefficients are used for facilities shielding design and to assess the radiation risk exposed population (Alghamdi et al., 2005; Bloch et al., 2016; Lopez Gonzalez et al., 2016). In actual situations the particle fluence can be measured and the conversion coefficients are used to transform the fluence to the required dosimetric quantity (Rogers, 1984; Santos et al., 2016). Conversion coefficients for neutrons, electrons and photons have been widely reported in literature (ANS, 1977; ICRU, 1998; ICRP, 2010).

2. Materials and methods

X-ray spectra and the dosimetric quantities were estimated using analog Monte Carlo method with the code MCNP5 (X-5 Monte Carlo Team, 2003). In this code the electron transport is modeled using the continuous slowing down approximation energy loss. In order to track an electron through a significant energy-loss, the electron path is broken in several steps that are picked short enough allowing that the mean energy loss is small, and long enough allowing several collisions. The Goudsmit-Saunderson theory (Goudsmit and Saunderson, 1940a, 1940b) is used to sample from the angular deflections distribution. The sampling of bremsstrahlung is addressed in every electron substep relaying mainly on the Bethe-Heitler theory (Bethe and Heitler, 1934). For improving the efficiency of electron and photon transport the code has two physics cards (PHYS:E and PHYS:P) that bias the production of secondary electrons by photons, the coherent scattering, the angular distribution of bremsstrahlung photons, and the production of characteristic X-rays. Thus, for photon transport the code includes coherent and Compton scattering as well as the bremsstrahlung production and

Table 1
Elements and densities of Monte Carlo model materials.

Item	Model elements	Density [g/cm^3]
Target	W	19.3
Glass	O, Na, Si, Ca	2.4
Air	N, O, Ar	1.205×10^{-3}
Lead shielding	Pb	11.35
Filter (Al_2O_3)	Al, O	3.987
Target axis	Cu	8.96

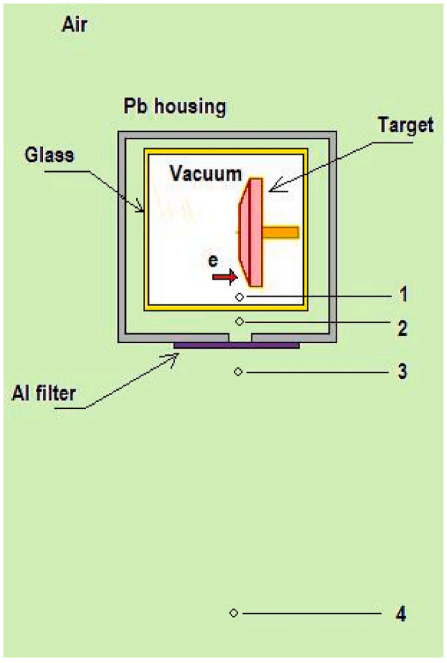

Fig. 1. Model of the X-ray tube.

the characteristic X-ray production after photoelectric absorption. (Ay et al., 2004).

The X-ray tube was modeled using the data of a commercial X-ray tube. In the model the target was built as tungsten truncated cone having an inclination of 21.8° encased in vacuum with 0.20 cm-thick glass (4 cm-radius). The X-ray tube is inside the 0.25 cm-thick lead housing (5 cm-radius) with a 0.75 cm-radius opening, below of this is the 0.28 cm-thick aluminum filter. In Table 1 are included the materials used to build the model.

A monoenergetic 0.028209 cm-radius electron beam (pencil-beam) was sent toward the tungsten target. The pencil-beam radius assures a 0.05×0.05 cm^2 focal spot. Calculations were carried out for 70, 80, 90, 100 and 120 keV monoenergetic electrons (Seibert and Boone, 2005; Seibert, 2004). The X-rays produced during the electron interactions were determined using the EL03 library for electrons (White, 2012) and the MCPLIB04 library for photons (Brown, 2013). Because this is an analog Monte Carlo calculation none variance reduction techniques were used.

Using tally f5 the X-ray spectra were estimated to 0.75 cm (between the target and the glass (position 1)), 2.25 cm (between the glass and the lead housing (position 2)), 3.75 cm (below the filter (position 3)), and to 100 cm (position 4) from the focal spot which is the site where electrons collide with the target. The spectra were estimated from 0 to 120 keV in 1 keV wide groups. In the calculations 2×10^8 histories were used allowing uncertainties less than 5%. In Fig. 1 is shown the X-ray tube model as well as the positions where the spectra were estimated.

To 1 m from the focal spot the X-ray spectrum ($\Phi_X(E)$) was used to calculate the Ka and the H*(10), per history, using the X-ray fluence-to-Air Kerma conversion coefficients (ka(E)) and the X-ray fluence–to-Ambient dose equivalent conversion coefficients (h*(E)) (ICRP, 1996), as is shown in equations (2) and (3). This calculation was made using the fm card for Ka and H*(10).

$$Ka = \int \Phi_X(E)\ ka(E)\ dE \tag{2}$$

$$H^*(10) = \int \Phi_X(E)\ h^*(E)\ dE \tag{3}$$

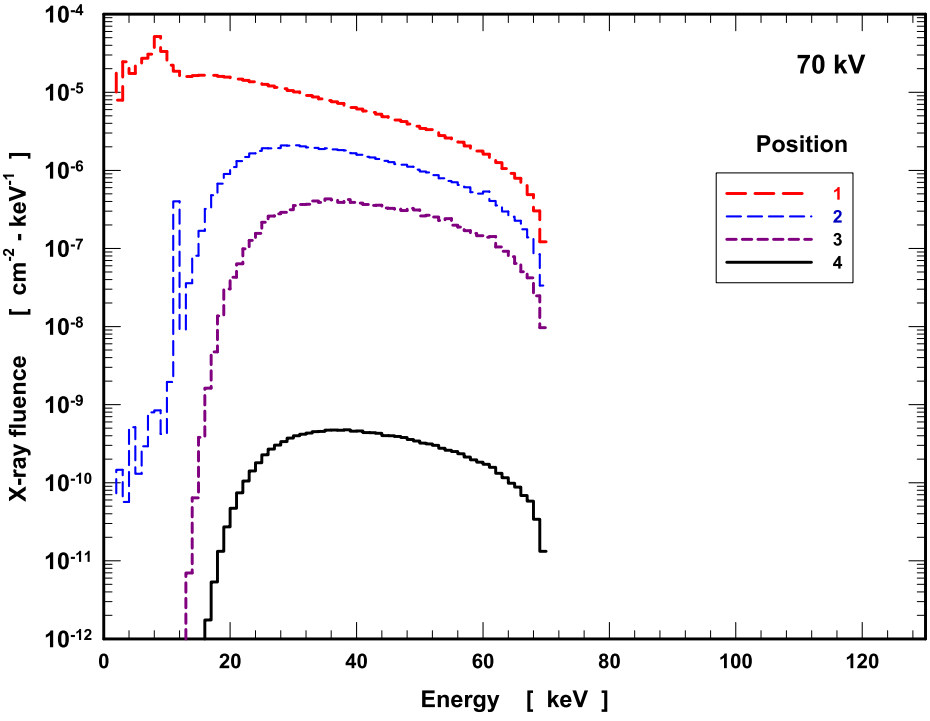

Fig. 2. X-ray spectra at positions 1, 2, 3, and 4, produced by the X-ray tube working to 70 kV.

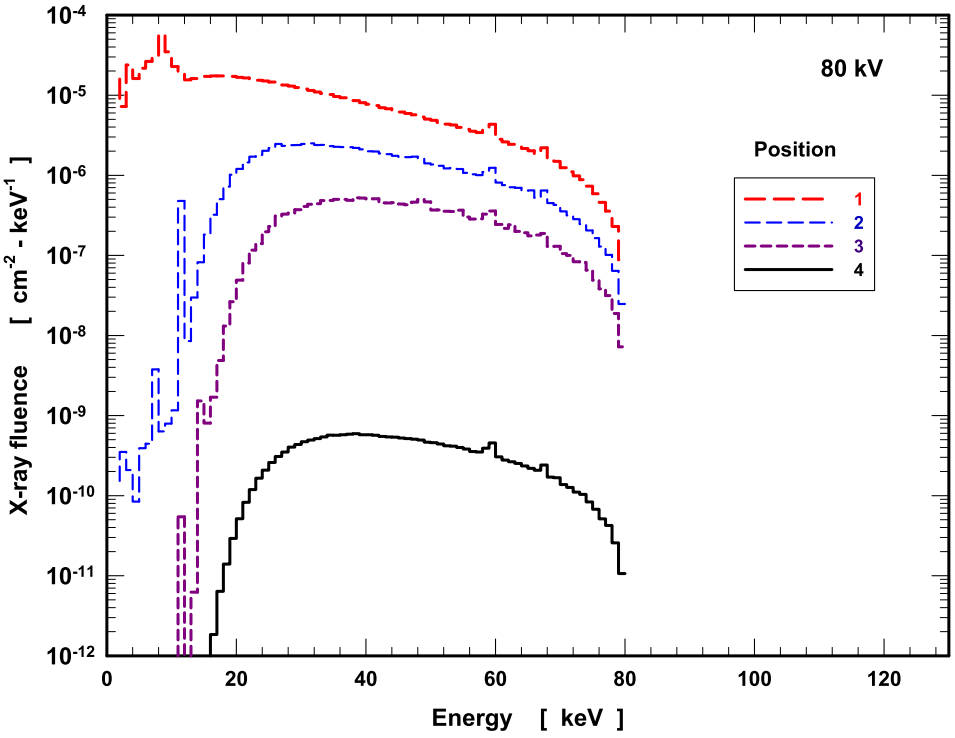

Fig. 3. X-ray spectra at positions 1, 2, 3, and 4, produced by the X-ray tube working to 80 kV.

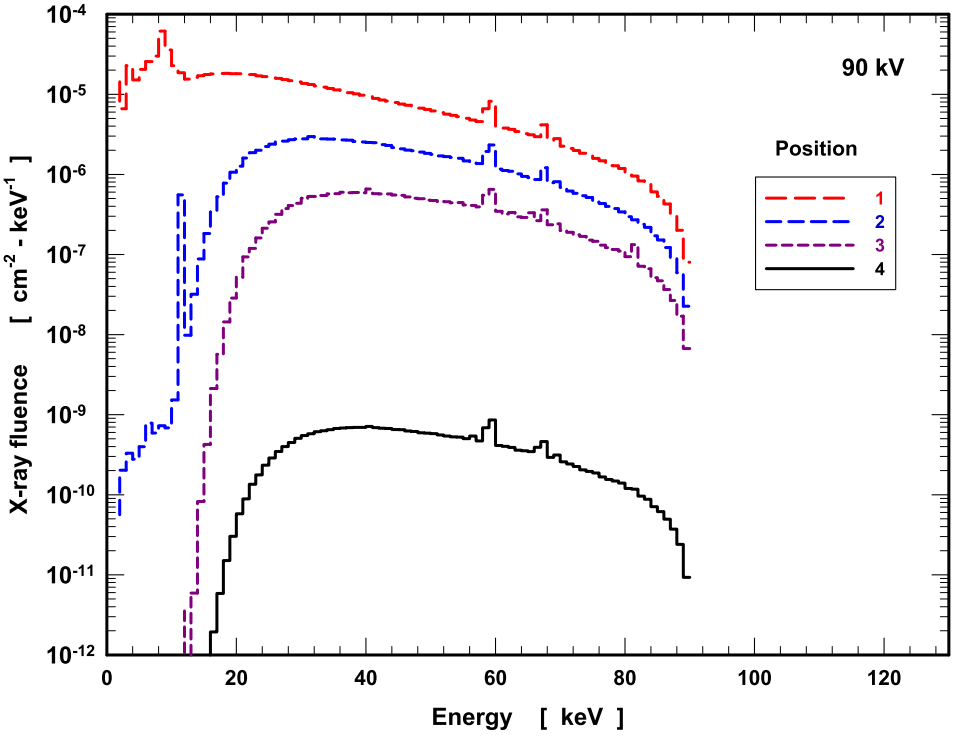

Fig. 4. X-ray spectra at positions 1, 2, 3, and 4, produced by the X-ray tube working to 90 kV.

Using equation (1), the Ka and H*(10) per history to 1 m, were used to calculate the Γ_{Ka} and the $\Gamma_{H^*(10)}$ factors in mA-min.

The mean energy of X ray spectra was estimated for each operation voltage; with the dosimetric quantities the Ka-to-H*(10) ratios were calculated. Also, the doses per unit photon fluence were calculated and compared with those for monoenergetic photons from the ICRP 74 (ICRP, 1996).

3. - results and discussion

In Figs. 2–6 are shown the photon spectra in position 1, 2, 3 and 4 for 70, 80, 90, 100, and 120 keV X-rays.

The end-energy of each spectrum is related to the voltage. In all cases the X-ray spectra in position 1 have the largest contribution of low energy photons, after reaching position 2 low energy photons are

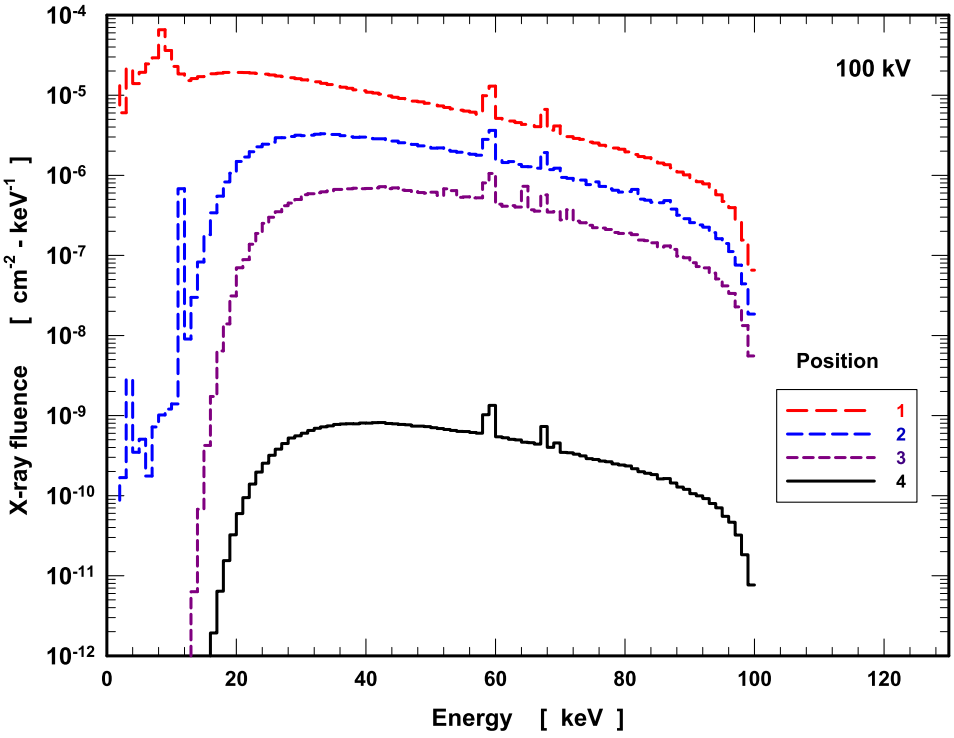

Fig. 5. X-ray spectra at positions 1, 2, 3, and 4, produced by the X-ray tube working to 100 kV.

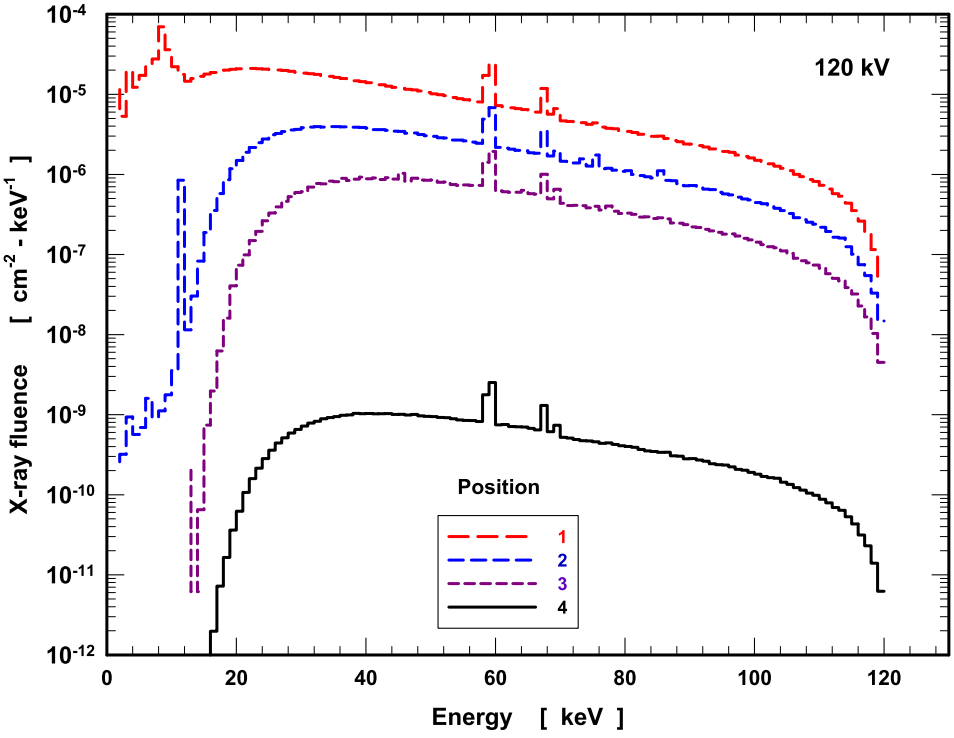

Fig. 6. X-ray spectra at positions 1, 2, 3, and 4, produced by the X-ray tube working to 120 kV.

attenuated by the glass and practically eliminated by the filter (position 3) (Boone and Siebert, 1997; Behrman and Yasuda, 1998).

The mean energy of X-ray spectra in position 1, 2, 3 and 4 are shown in Table 2.

The spectra mean energies increase as the voltage increases and as the site-to-focal spot distance increases, being in agreement with the evidence shown in Figs. 2–6 where glass and filter eliminate the low energy photons resulting in harder spectra (Boone and Siebert, 1997; Behrman and Yasuda, 1998).

In Fig. 7 are shown the X-ray spectra in position 4 for 70, 80, 90, 100 and 120 kV whose mean energies are 42.4, 45.9, 49.1, 52.0 and 57.2 keV respectively.

For all voltages, except for 70 kV, the spectra show the $K_{\alpha 1}$ (59.32 keV), $K_{\alpha 2}$ (57.98 keV), $K_{\beta 1}$ (67.24 keV) and $K_{\beta 2}$ (69.1 keV) characteristic

Table 2
Photons mean energy, in keV, of 70, 80, 90, 100 and 120 kV X-ray spectra in positions 1, 2, 3, and 4.

Position	70 kV	80 kV	90 kV	100 kV	120 kV
1	20.8	23.5	26.4	29.3	34.7
2	37.4	40.4	43.3	46.2	51.0
3	42.1	45.4	48.5	51.5	56.4
4	42.4	45.9	49.1	52.0	57.2

X-rays which are due to tungsten, while for all voltages the spectra have the continuous contribution due to Bremsstrahlung photons, being in agreement with spectra reported in literature (Boone and Siebert, 1997; Bath et al., 1998; Lopez Gonzalez et al., 2016). The lack of characteristic X-rays in the 70 kV-spectrum is probably due to low amount of 57.98, 59.32, 67.24 and 69.1 keV photons and the low probability of interaction between resonant photons and the tungsten K shell.

The $\Gamma_{H^*(10)}$ and Γ_{Ka}, are shown in Table 3, also is included the Ka-to-H*(10) ratios. These values increase as the voltage increases. The Γ_{Ka}, are in agreement with measurements reported by Katoh et al. (2011) for 70, 80, 90, 100 and 120 kV X-ray tubes with inverter type high-voltage generator. The $\Gamma_{H^*(10)}$ factor are very close to the values recommended by the German norm (DIN, 2013) while the Γ_{Ka} are close to values reported by the ICRP 33 (ICRP, 1982), and those reported by Poludniowski (2007). Also, the Ka-to-H*(10) ratios are alike those reported by Lopez Gonzalez et al. (2016) and Santos et al. (2016) in function of the mean energy of X-ray spectra.

Fluence-to-dose conversion coefficients are the dose divided by the total fluence, here the Ka and the H*(10) were divided by the total photon fluence in order to obtain the X-ray fluence-to-Air Kerma coefficient (ka_X) and the X-ray fluence-to-Ambient dose equivalent (h^*_X). These values are shown in Table 4.

In Fig. 8 the ka_X and h^*_X coefficients were compared with the fluence-to-dose conversion coefficients for monoenergetic photons (ICRP, 1996). In order to make this comparison both ka_X and h^*_X, were plotted in terms to the mean energy of the X-ray spectrum (Table 1, position 4).

Conversion coefficients for X-rays are larger than those of monoenergetic photons. In the spectra photons have a broad energy distribution characterized by their mean energy. In the interaction with matter photons with lower energy have a larger probability of being absorbed through the photoelectric effect and their energy is absorbed, for photons with larger energies the probability of photoelectric interaction decreases and the probability of Compton scattering increases where just part of the photon energy is absorbed and the scattered photon can escape.

4. Conclusions

The X-ray spectra were estimated and the Γ factors for Ka and H*(10) were calculated for X-ray tubes working to 70, 80, 90, 100 and 120 kV.

Table 3
$\Gamma_{H^*(10)}$, Γ_{Ka} factors and Ka-to-H*(10) ratios.

Voltage [kV]	$\Gamma_{H^*(10)}$ [mSv-m^2/mA-min]	Γ_{Ka} [mGy-m^2/mA-min]	H*(10)/Ka [Sv/Gy]
70	3.49 ± 0.01	2.67 ± 0.01	1.31
80	4.85 ± 0.01	3.57 ± 0.01	1.36
90	6.44 ± 0.02	4.60 ± 0.01	1.40
100	8.22 ± 0.01	5.73 ± 0.01	1.43
120	12.09 ± 0.02	8.17 ± 0.01	1.48

Table 4
X-ray fluence to 1 m, fluence-to-H*(10) and fluence-to-Ka conversion coefficients.

Voltage [kV]	X-ray fluence to 1 m [photons/cm^2-mA-min]	h^*_X [pSv-cm^2]	ka_X [pGy-cm^2]
70	(5.291 ± 0.012)E(09)	0.660 ± 0.002	0.505 ± 0.002
80	(7.626 ± 0.015)E(09)	0.636 ± 0.002	0.468 ± 0.002
90	(1.039 ± 0.004)E(10)	0.620 ± 0.003	0.443 ± 0.002
100	(1.349 ± 0.002)E(10)	0.609 ± 0.001	0.425 ± 0.001
120	(2.016 ± 0.003)E(10)	0.600 ± 0.001	0.405 ± 0.001

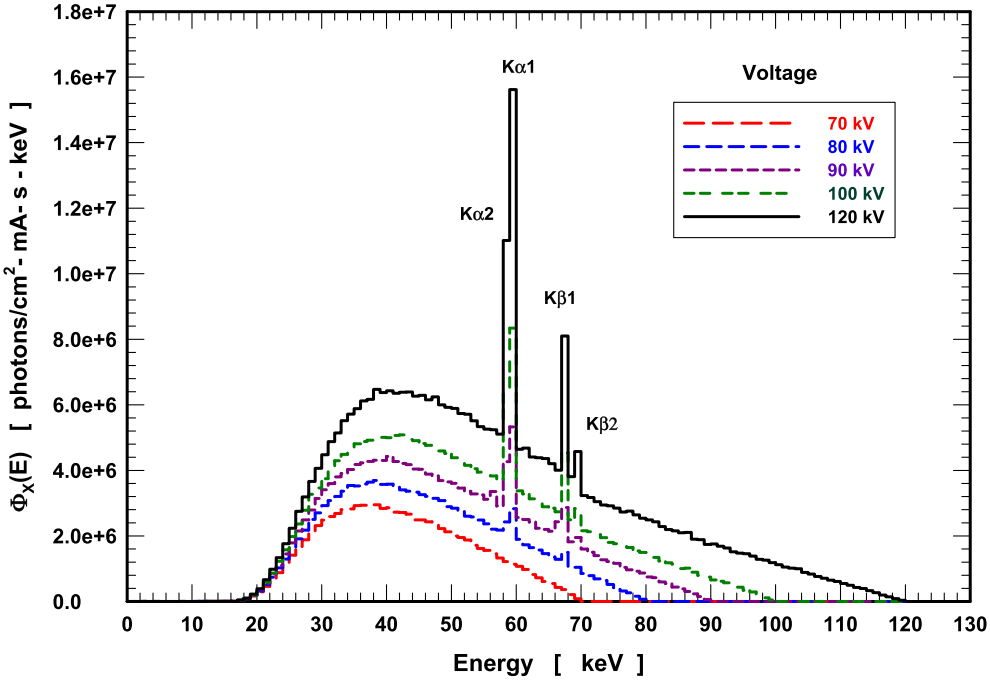

Fig. 7. X-ray spectra to 1 m from the focal spot (position 4), for 70, 80, 90, 100 and120 kV X-ray tubes.

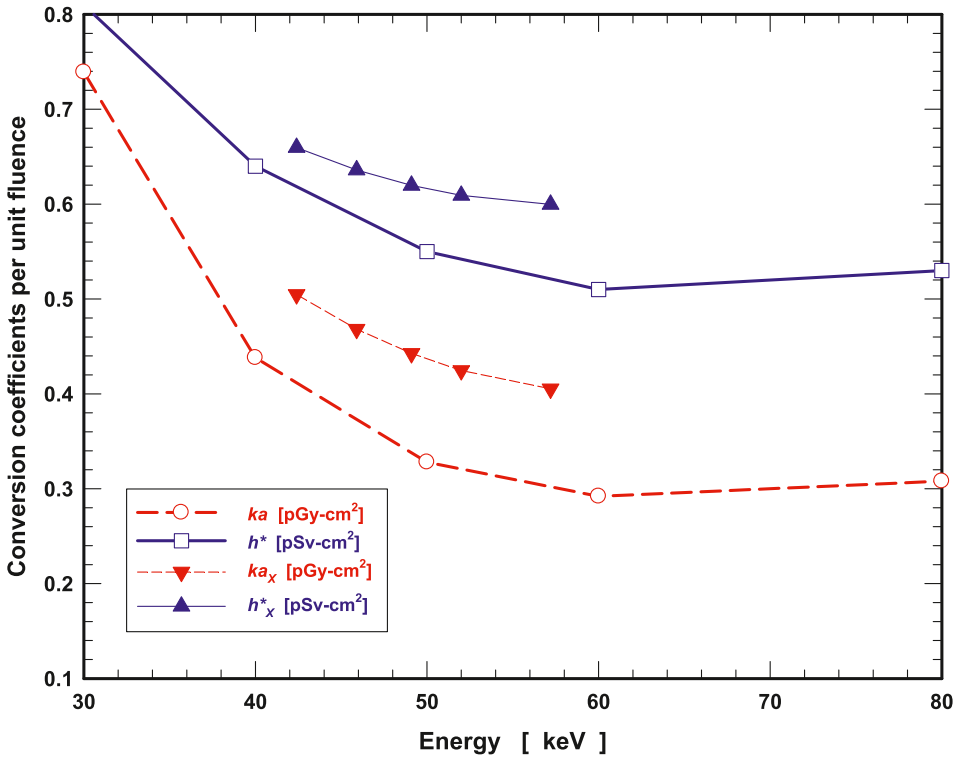

Fig. 8. Ka and H*(10) conversion coefficients per unit fluence for monoenergetic photons (ka and h*) and for 70, 80, 90, 100 and 120 keV X-rays (ka_X and h^*_X).

The total photon fluence, the Ka-to-H*(10) ratios and the ka_X and h^*_X conversion coefficients were calculated and compared with those of monoenergetic photons.

The X-ray spectra are modified as photon pass through the glass and the filter where photons are absorbed.

X rays have the continuous spectra due to Bremsstrahlung where the end-energy is the operation voltage. The discrete spectra show 4 peaks which are characteristic to the tungsten target and are noticed for 80–120 kV.

For 70 kV the discrete spectrum is absent because there are few resonant photons with the energy to ionize K-shell electrons in the tungsten target.

To 1 m from the focal spot the Γ_{Ka} is 8.17 mGy-m^2-mA^{-1}-min^{-1}, and the $\Gamma_{H^*(10)}$ is 12.09 mSv-m^2-mA^{-1}-min^{-1}.

The ka_X and the h^*_X are larger than the conversion coefficients per unit fluence for monoenergetic photons.

Author statment

Any data will be available upon request.

Declaration of competing interest

Authors declare that as far as we know there is not any competing interests (financial, academic or scientific) neither personal relationship that could have appeared to influence the work here reported.

Acknowledgments

First to fifth authors thanks to CONACyT (Mexico) for the scholarship granted to pursue their postgraduate degrees.

References

Alghamdi, A.A., Ma, A., Tzortzis, Spyrou, N.M., 2005. Radiat. Protect. Dosim. 115, 606–611. https://doi.org/10.1093/rpd/nci268.

Ans, 1977. American National Standard: Neutron and Gamma-Ray Flux-To-Dose-Rate Factors. ANS/ANS 6.1.1-1997. American Nuclear Society, La Grange Park IL (USA).

Ay, M.R., Shahriari, M., Sarkar, S., Adib, M., Zaidi, H., 2004. Monte Carlo simulation of x-ray spectra in diagnostic radiology and mammography using MCNP4C. Phys. Med. Biol. 49, 4897–4917. https://doi.org/10.1088/0031-9155/49/21/004.

Behrman, R.H., Yasuda, G., 1998. Effective dose in diagnostic radiology as a function of x-ray beam filtration for a constant exit dose and constant film density. Med. Phys. 25, 780–790. https://doi.org/10.1118/1.598260.

Bethe, H.A., Heitler, W., 1934. On stopping of fast particles and on the creation of positive electrons. Proc. Roy. Soc. Lond. A 146, 83–112. https://doi.org/10.1098/rspa.1934.0140.

Bhat, M., Pattison, J., Bibbo, G., Caon, M., 1998. Diagnostic x-ray spectra: a comparison of spectra generated by different computational methods with a measured spectrum. Med. Phys. 25, 114–120. https://doi.org/10.1118/1.598170.

Birch, R., Marshall, M., 1979. Computation of bremsstrahlung X –ray spectra and comparison with spectra measured with a Ge(Li) detector. Phys. Med. Biol. 24, 505–517. https://doi.org/10.1088/0031-9155/24/3/002.

Blakely, E.A., 2000. Biological effects of Cosmic radiation: deterministic and stochastic. Health Phys. 79, 495–506. https://doi.org/10.1097/00004032-200011000-00006.

Bolch, W.E., Petoussi-Henss, N., Paquet, F., Harrison, J., 2016. ICRP dose coefficients: computational development and current status. Ann. ICRP 45, 156–177.

Boone, J.M., 1998. The three parameter equivalent spectra as an index of beam quality. Med. Phys. 15, 304–310. https://doi.org/10.1118/1.596223.

Boone, J.M., Siebert, J.A., 1997. An accurate method for computer-generating tungsten anode x-ray spectra from 30 to 140 kV. Med. Phys. 24, 1661–1670. https://doi.org/10.1118/1.597953.

Brown, F., 2013. Status of Cross-Section Data Libraries for MCNP. Los Alamos National Laboratory technical report LA-UR-13-23040.

Campillo-Rivera, G.E., Vazquez-Bañuelos, J., Garcia-Duran, A., Escalona-Llaguno, M.I., Vasquez Arteaga, M., Vega-Carrillo, H.R., 2019. Dose in eye lens, thyroid, salivary glands, mammary glands, and gonads, due to radiation scattered in dental orthopantomography. Appl. Radiat. Isot. 146, 57–60. https://doi.org/10.1016/j.apradiso.2019.01.022.

Cheol-Ha, B., Seung-Jae, L., Kim, D., 2018. Diagnostic X-ray spectra detection by Monte Carlo simulation. J. Korean Soc. Radiol. 12, 289–295. https://doi.org/10.7742/JKSR.2018.12.3.289.

Dewji, S.A., Hertel, N.E. (Eds.), 2019. Advanced Radiation Protection Dosimetry. CRC Press, Boca Raton, Fl (USA).

DIN, 2013. Medical X-Ray Equipment up to 300 kV-Rules of Construction for Structural Radiation Protection. DIN 6812 German Institute for Standardization.

Gauvin, R., Michaud, P., 2009. MC X-Ray, a new Monte Carlo program for quantitative X-ray microanalysis of real materials. Microsc. Microanal. 15, 488–489. https://doi.org/10.1017/S1431927609092423.

Gauvin, R., Lifshin, E., Demers, H., Horny, P., Campbell, H., 2006. Win X-ray: a new Monte Carlo program that computes X-ray spectra obtained with a scanning electron microscopy. Microsc. Microanal. 12, 49–64. https://doi.org/10.1017/S1431927606060089.

Goudsmit, S., Saunderson, J.L., 1940a. Multiple scattering of electrons. Phys. Rev. 57, 24–29. https://doi.org/10.1103/PhysRev.57.24.
Goudsmit, S., Saunderson, J.L., 1940b. Multiple scattering of electrons II. Phys. Rev. 58 https://doi.org/10.1103/PhysRev.58.36, 58-42.
Holroyd, J., 2018. Measurement of scattered and transmitted x-rays from intra-oral and panoramic dental x-ray equipment. J. Radiol. Prot. 38, 793–806. https://doi.org/10.1088/1361-6498/aabce3.
ICRP, 1982. Protection against ionizing radiation from external sources used in medicine. ICRP publication 33. Ann. ICRP 9.
ICRP, 1991. 1990 recommendations of the international commission on radiological protection. ICRP 60. Ann. ICRP 21, 32–49.
ICRP, 1996. Conversion coefficients for use in radiological protection against external radiation. ICRP 74. Ann. ICRP 26, 159–179.
ICRP, 2010. Conversion coefficient for Radiological protection quantities for external radiation exposures. ICRP 116. Ann. ICRP 40.
ICRU, 1998. Conversion coefficients for use in Radiological Protection against external radiation. ICRU 57. J. ICRU 29.
Katoh, Y., Mita, S., Fukushi, M., Nyui, Y., Abe, S., Kimura, J., 2011. Calculation of air-kerma rate of diagnostic X-ray generators. Radiol. Phys. Technol. 4, 1–6. https://doi.org/10.1007/s12194-010-0097-7.
Lopez-Gonzales, A.H., Santos, J.C., Mariano, L., Tomal, A., Costa, P.R., 2016. Evaluation of mean conversion coefficients from air-kerma to H*(10) using secondary and transmitted x-ray spectra in the diagnostic radiology energy range. J. Radiol. Prot. 36, 842–857. https://doi.org/10.1088/0952-4746/36/4/842.
NCRP, 1993. Limitation of Exposure to Ionizing Radiation. NCRP Report No. 116. National Council on Radiation Protection and Measurements, Bethesda, MD.
NCRP, 2003. Radiation Protection in Dentistry. NCRP Report No. 145. National Council on Radiation Protection and Measurements, Bethesda, MD.
NCRP, 2004. Structural Shielding Design for Medical X Ray Imaging Facilities. NCRP Report No. 147. National Council on Radiation Protection and Measurements, Bethesda, MD.
Ninkovic, M.M., Raicevic, J.J., Adrovic, F., 2005. Air kerma rate constants for gamma emitters used most often in practice. Radiat. Protect. Dosim. 115 (1–4), 247–250. https://doi.org/10.1093/rpd/nci131.
NOM, 2006. Norma oficial mexicana NOM-229-SSA1-2002. http://www.economia-noms.gob.mx/normas/noms/2006/229ssa1.pdf.
Okunade, A.A., 2005. Effective dose as a limiting quantity for the evaluation of primary barriers for diagnostic X-ray facilities. Health Phys. 89, S100–S116. https://doi.org/10.1097/00004032-200511005-00011.
Omar, A., Andreo, P., Poludniowski, G., 2020a. A model for the energy and angular distribution of x rays emitted from an x-ray tube. Part I. Bremsstrahlung production. Med. Phys. 47, 4763–4774. https://doi.org/10.1002/mp.14359.
Omar, A., Andreo, P., Poludniowski, G., 2020b. A model for the energy and angular distribution of x rays emitted from an x-ray tube. Part II. Validation of x-ray spectra from 20 to 200 kV. Med. Phys. 47, 4005–4019. https://doi.org/10.1002/mp.14360.
Omori, Y., Hosoda, M., Takahashi, F., Sanada, T., Hirao, S., Ono, K., Furukawa, M., 2020. Japanese population dose from natural radiation. J. Radiol. Prot. 40, R99–R140. https://doi.org/10.1088/1361-6498/ab73b1.
Pibida, L., Minniti, R., Lucas, L., Seltzer, S.M., 2008. The Air-Kerma rate constants: application to air-kerma measurements for homeland security. Health Phys. 94, 126–133. https://doi.org/10.1097/01.HP.0000285799.20091.d8.
Poludniowski, G.G., 2007. Calculation of x-ray spectra emerging from an x-ray tube. Part II. X-ray production and filtration in x-ray targets. Med. Phys. 34, 2175–2186. https://doi.org/10.1118/1.2734726.
Poludniowski, G., Landry, G., DeBlois, F., Evans, P.M., Verhaegen, F., 2009. SpeakCalc: a program to calculate photon spectra from tungsten anode x-ray tubes. Phys. Med. Biol. 54, N433–N438. https://doi.org/10.1088/0031-9155/54/19/N01.
Rodriguez-Ibarra, J.L., Hernandez-Adame, P.L., Vega-Carrillo, H.R., Rivera, T., 2016. X-ray spectra and doses. Appl. Radiat. Isot. 117, 32–35. https://doi.org/10.1016/j.apradiso.2016.04.001.
Rogers, D.W.O., 1984. Fluence to dose equivalent conversion factors calculated with EGS3 for electrons from 100 keV to 20 GeV and photons from 11 keV to 20 GeV. Health Phys. 46, 891–914. https://doi.org/10.1097/00004032-198404000-00015.
Santos, J.C., Mariano, L., Tomal, A., Costa, P.R., 2016. Evaluation of conversion coefficients relating air-kerma to H*(10) using primary and transmitted x-ray spectra in the diagnostic radiology energy range. J. Radiol. Prot. 36, 117–132. https://doi.org/10.1088/0952-4746/36/1/117.
Sechopoulos, I., Ali, E.S.M., Badal, A., Badano, A., Boone, J.M., Kyprianou, I.S., Mainegra-Hing, E., McMillan, K.L., McNitt-Gray, M.F., Rogers, D.W.O., Samei, E., Turner, A.C., 2015. Monte Carlo reference data sets for imaging research: executive summary of the report of AAPM Research Committee Task Group 195. Med. Phys. 42, 5679–5691. https://doi.org/10.1118/1.4928676.
Sechopoulos, I., Rogers, D.W.O., Bazalova-Carter, M., Bloch, W.E., Heath, E.C., McNitt-Gray, M.F., Sempau, J., Williamson, J.F., 2018. RECORDS: improved reporting of Monte Carlo RaDiation transport studies: report of the AAPM research committee task group 268. Med. Phys. 45, e1–e5. https://doi.org/10.1002/mp.12702.
Seibert, J.A., 2004. X-ray imaging physics for Nuclear Medicine technologists. Part 1: basic principles of X-ray production. J. Nucl. Med. Technol. 32, 139–147.
Seibert, J.A., Boone, J.M., 2005. X-ray imaging physics for Nuclear Medicine technologists. Part 2: X-ray interactions and image formation. J. Nucl. Med. Technol. 33, 3–18.
Shafahi, Z., Sina, S., Faghihi, R., 2020. Comparison of TSVD, MTSVD, and Tiknonov unfolding methods for reconstruction of X-ray spectra. Radiat. Phys. Chem. 166, 108437 https://doi.org/10.1016/j.radphyschem.2019.108437.
Smith, D.S., Stabin, M.G., 2012. Exposure rate constants and lead shielding values for over 1,100 radionuclides. Health Phys. 102, 271–291. https://doi.org/10.1097/HP.0b013e318235153a.
Teles, P., Trincao, M., Alves, F., Antunres, V., Calado, D., Cantinho, G., Carvalho, A.L., Domingues, A., Geao, A., Godinho, F., Isidoro, J., Lanca, I., Líbano, L., Loureiro, M. F., Macedo, R., Moreira, R., Neves, D., Pereira, E., Pimenta Marinho, A., Pintao, S., Robalo, J., Santos, J., Santos, J.A.M., Silva, M., Silveira, J., Simaozinho, P., Teixeira, S., Vale, J., Vaz, A.F., Vaz, P., 2020. Evaluation of the Portuguese population exposure to ionizing radiation due to x-ray and nuclear medicine procedures from 2013 to 2017. Radiat. Phys. Chem. 172, 108762. https://doi.org/10.1016/j.radphyschem.2020.108762, 2020.
Ungar, L.M., Truby, D.K., 1982. Specific Gamma Ray Dose Constants for Nuclides Important to Dosimetry and Radiological Assessment. Report No. ORNL/RSIC- 45/R1. Oak Ridge National Laboratory, Oak Ridge TN, USA.
Vazquez-Bañuelos, J., Campillo-Rivera, G.E., Garcia-Duran, A., Reyes Rivera, E., Vasquez Arteaga, M., Baltazar Raigosa, A., Vega-Carrillo, H.R., 2019. Doses in eye lens, thyroid, and gondas, due to scattered radiation, during a CT radiodiagnosis study. Appl. Radiat. Isot. 147, 31–34. https://doi.org/10.1016/j.apradiso.2019.02.012.
Wasserman, H., Groenwald, W., 1988. Air kerma rate constants for radionuclides. Eur. J. Nucl. Med. 14, 569–571. https://doi.org/10.1007/BF00286779.
Webster, E.W., 1995. X rays in diagnostic radiology. Health Phys. 69, 610–635. https://doi.org/10.1097/00004032-199511000-00001.
White, M.C., 2012. Further Notes on MCPLIB03/04 and New MCPLIB63/84 Compton Broadening Data for All Versions of MCNP5. Technical Report LA-UR-12-00018. Los Alamos National Laboratory.
Willemink, M.J., Koszek, W.A., Hardell, C., Wu, J., Fleischmann, D., Harvey, H., Folio, L. R., Summers, R.M., Rubin, D.L., Lungren, M.P., 2020. Preparing medical imaging data for machine learning. Radiology 295, 4–15. https://doi.org/10.1148/radiol.2020192224.
X-5 Monte Carlo Team, 2003. MCNP-A General Monte Carlo N-Particle Transport Code, Version 5. LA-UR-03-1987. Los Alamos National Laboratory.